Ultrasonic Lamb wave inspection of composite defects

Zhaoyun Ma, Lingyu Yu
Department of Mechanical Engineering, University of South Carolina
Columbia, SC, USA
zhaoyun@email.edu , yu3@cec.sc.edu

ABSTRACT

Composites have been extensively used in aerospace engineering due to their advantages of light weight, high strength, and engineering design flexibility. Manufacturing defects such as wrinkle and porosity can affect the performance of the composites and may lead to failure in the end, while damage such as delamination, fiber fraction, and matrix cracking can directly cause failure of the composites. In this paper, a Lamb wave based nonintrusive nondestructive evaluation system, which employs piezoelectric transducer for actuation and scanning laser Doppler vibrometer for wavefield sensing, is presented for typical composite defect and damage inspection and evaluation. Two composite panels with different geometry (flat or curved) and with various embedded defects (wrinkle and delamination) are inspected using the nonintrusive Lamb wave system. Both the wrinkles and delamination are detected from the wavefield and approximately quantified through wavefield imaging methods.

Keywords: wrinkles, delamination, Lamb waves, nonintrusive inspection, laser vibrometer

1 INTRODUCTION

Composites have been extensively used in aerospace engineering since they are light weight and flexible for engineering design. In recent years, composites have become the predominant components in the new airframes instead of traditionally used metal material such as aluminum. However, manufacturing defects such as wrinkle and porosity can affect the performance of the composites which may lead to failure in the end, while damage such as delamination, fiber fraction, and matrix cracking can directly cause failure of the composites. Thus, early detection of those defects and damage using effective nondestructive evaluation (NDE) methods is crucial to ensure the structure safety and reliability.

Lamb wave based NDE methods have been proven effective for damage detection and quantification in composite structures [1-7]. Research includes that has been conducted by Park et al. which demonstrated Lamb wave based active sensing using time reversal technique on a pristine composite plate to achieve reference-free damage inspection [1]. Purekar and Pines presented Lamb wave inspection capability on a composite laminate with inter-ply delamination using piezoelectric sensor arrays [2]. Sohn et al. conducted automated inspection on a composite plate with delamination and disbond and detected them through Lamb wave wavefield imaging methods [3]. Juarez and Leckey performed Lamb wave based wavenumber analysis and correlated the impact delamination to ply numbers of a composite plate [5]. Tian et al utilized multidimensional Lamb wavefield analysis on a composite plate and quantified the impact delamination inside the structure [6]. Most of these research focuses on Lamb wave methods development and their application on flat composite panels with delamination. Lamb wave based inspection on composite plates with complex geometries or other defects and/or damage are less studied and reported to the best knowledge of authors.

This paper aims to evaluate the capability of Lamb wave based NDE methods on composite panels with different geometries and with various embedded defects such as wrinkle, and damage such as delamination. A nonintrusive piezoelectric transducer-scanning laser Doppler vibrometer (PZT-SLDV) Lamb wave NDE system is employed. Honey is used as PZT couplant instead of traditional adhesive while wipe off reflective spray is applied as surface light enhancement instead of reflective tape. Two composite panels with different geometry (flat or curved) and defects (wrinkles and delamination) are inspected. Defects and damage are further evaluated and visualized through wavefield imaging methods. The systematic case studies on composite panels with Lamb wave based NDE methods will enable rapid inspection and health monitoring methods towards new composite structural systems.

2 NONINTRUSIVE LAMB WAVE INSPECTION METHODS

PZT-SLDV Lamb wave system has been implemented in damage detection in previous research and has been proven its capability and reliability [7-10]. In this section, a non-intrusive PZT-SLDV system is first established by using honey as couplant for Lamb wave actuation and wipe-off reflective spray for SLDV wavefield sensing enhancement. A rapid and straightforward wavefield imaging method is adopted and presented using the PZT-SLDV actuated and measured Lamb wave wavefield data.

2.1 Nonintrusive PZT-SLDV experimental setup

The PZT-SLDV Lamb wave inspection system is implemented to inspect the target composite panels. The system employs contact type PZT as actuator to excite Lamb waves in the testing plate [5]. Traditionally the PZT is bonded on the surface of specimen using adhesive, and it can generate Lamb waves by coupling its in-plane motion with the structure through the adhesive layer [1]. For the Lamb wave sensing and visualization, noncontact, rapid and high-spatial-resolution SLDV is employed. SLDV is capable of scanning a predefined area by directing the laser beam to multiple points. Displacement or velocity of the particle motion is measured along the laser beam based on the Doppler effect. However, reflective tape is generally attached on the specimen surface for light reflection enhancement, especially for composite material with less reflective surface properties. Removing the PZT or the tape are time and labor consuming and will likely modify the condition of the sample surface. Hence, in the subject inspection completely non-invasive PZT-SLDV installation and setup are implemented, using honey as couplant for PZT actuation and wipe-off reflective spray for SLDV signal enhancement.

The overall laboratory experimental setup of the PZT-SLDV system is illustrated in Figure 1. A Tektronix AFG3022C arbitrary waveform generator is used to excite the selected excitation signal to the actuator PZT. Through in-plane piezoelectric coupling, guided waves are excited in the testing plates, a.k.a. Lamb waves. To improve the signal strength and quality, a bipolar amplifier (NF HSA 4014) is employed to magnify the excitation signal strength. For the sensing part, the SLDV head is placed normal to the specimen surface so that only the out-of-plane surface particle velocity will be measured in the predefined scanning line or area.

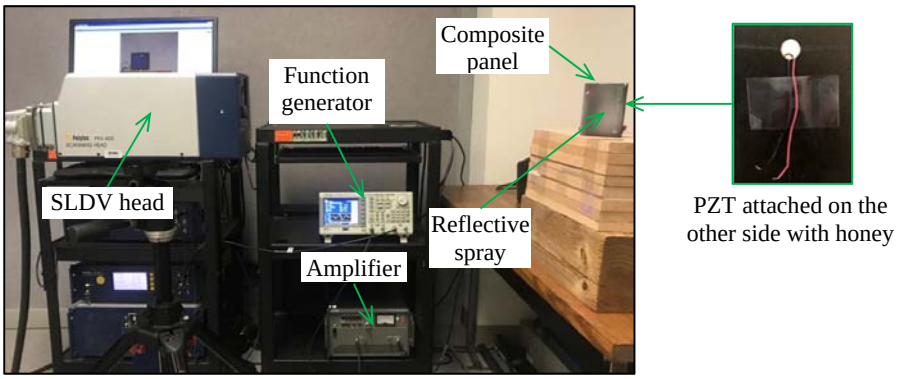

Figure 1 Nonintrusive PZT-SLDV Lamb wave inspection system experimental setup

2.2 Wavefield imaging method

Using the PZT-SLDV Lamb wave inspection system, multidimensional time-space Lamb wave wavefield $v(t,\mathbf{x})$ in terms of time t and space $\mathbf{x}$ is obtained, where $\mathbf{x}$ represents the space vector (x,y) of each predefined scanning point. Using the wavefield data, wave propagation videos or wavefield snapshots at certain time can be directly acquired, where the wave damage interactions can be observed immediately, indicating that structural discontinuity may exist [11, 12]. However, it is difficult to quantify the damage from the wavefield itself by human naked eyes, and often requires comprehensive understanding of Lamb wave signatures and the characteristics they interact with different types of damage. Thus, a distributed energy field image that can visualize and quantify the damage more intuitively is generated in this paper by calculating the peak amplitude of the recorded waveform at each scanning point as:

$$v^{mag}(\mathbf{x}) = \max\left(\left|v(t,\mathbf{x})\right|\right) \tag{1}$$

3 INSPECTION ON TWO TYPICAL COMPSOTE DEFECT AND DAMAGE

With the presented nonintrusive PZT-SLDV inspection system accompanied with wavefield imaging methods presented in Section 2, two types of typical composite defect and damage are inspected and evaluated in this section: case 1 wrinkles in a flat composite panel, and case 2 multiple embedded delamination in a curved composite panel. The relevant inspection schemes and evaluation results are presented in the following.

3.1 Case 1: wrinkle inspection

A flat composite panel with wrinkle defects manufactured by Boeing as shown in Figure 2 is inspected in this case. The measured dimension of the panel is 306 × 260 × 3.83 (unit: mm). Significant wrinkles are observed on both the top and bottom surfaces of the plate (pointed by red arrows in Figure 2a and Figure 2b). Cartesian coordinates are used with the origin set at the left bottom corner on the top surface. The thickness view of the plate is shown in Figure 2c. The area with more wrinkles (0-160 mm along *x* direction) is defined as wrinkle region while the part with less wrinkles (160-306 mm along *x* direction) is defined as reference region. Note the bottom side picture of the plate is flipped horizontally to match the wrinkle distribution along *x* direction as well as share the same coordinates used on top surface.

The inspection schematics are shown in Figure 2d. The predefined wrinkle region is marked as red while the reference region is marked as green. The PZT actuator is attached at O_1 (160, 115) in order to interrogate both the two regions. A 3-count toneburst at 240 kHz amplified to 50 V_{pp} is used as excitation. The scanning is performed in the area 100 mm by 50 mm with 1-mm spatial resolution and 30 averages are used to improve the SLDV signal to noise ratio. VD-07 velocity decoder with measurement 10 mm/s/V is selected for measuring signals with frequency up to 350 kHz. Note the inspection is performed on the top side of the plate. Inspections are also performed with the PZT attached at other two locations O_2 and O_3 as shown in Figure 2 in order to create different inspection perspectives. The scanning area is 140 mm by 50 mm with PZT at O_2 for wrinkle region inspection while 120 mm by 50 mm with PZT at O_3 for reference region inspection.

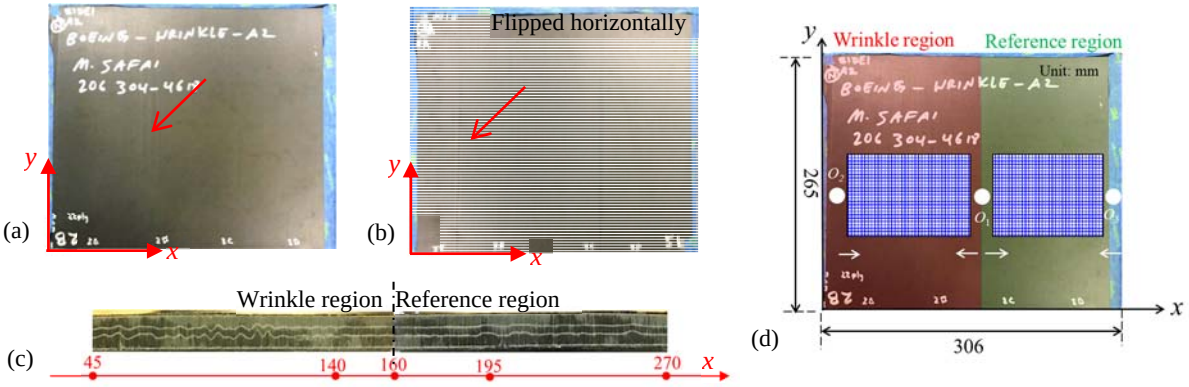

Figure 2 The tested composite panel with wrinkles: (a) top surface view, (b) bottom surface view, and (c) thickness view; (d) inspection actuation and sensing schemes with PZT attached at O_1, O_2, and O_3

The measured wavefields with PZT at location O_1 for wrinkle and reference region inspection are plotted in Figure 3. Mode conversion is observed in both wavefields, indicating structural discontinuity existence. The circular wavefront of the Lamb waves are modified to straight crested waves which guided by the wrinkle defect straight pattern. In addition, a faster wave mode which is believed to be S_0 is observed in the reference region wavefield while not in the wrinkle region. This indicates that likely less wrinkle defects exist in the reference region so that some of the S_0 waves transmitted through, while more wrinkles in the wrinkle region and the S_0 mode are all mode converted to A_0 mode. In order to quantify the wrinkles, energy based field images are generated using Eq. (1) and presented in Figure 4. Clear wrinkle patterns are observed in both images for wrinkle and reference region: 55 mm (85 mm to 140 mm) for wrinkle region and 25 mm (185 mm to 210 mm) for reference region respectively. Note that the wrinkles pattern can also be the converted wave mode patterns from circular wavefront to straight wavefront. Considering the source location, we can conclude that the wrinkle defect boundaries are x=140 mm for wrinkle region and x=210 mm for reference region, which matches the visual inspection from the thickness view (Figure 2c). The inspection results with PZT at O_2 for wrinkle region inspection and at O_3 for reference region inspection are shown in Figure 5. The wrinkle starts at about 50 mm for wrinkle region, while wrinkles exist in the ranges from 180 to 210 mm and at about 250 mm for reference region. Combining all the inspection

results, it can be concluded that the wrinkle defects exist from 50 to 140 mm for wrinkle region and from 180 to 210 mm and at 250 mm for reference region. The final inspection results agree well with the visual inspection results shown in Figure 2c.

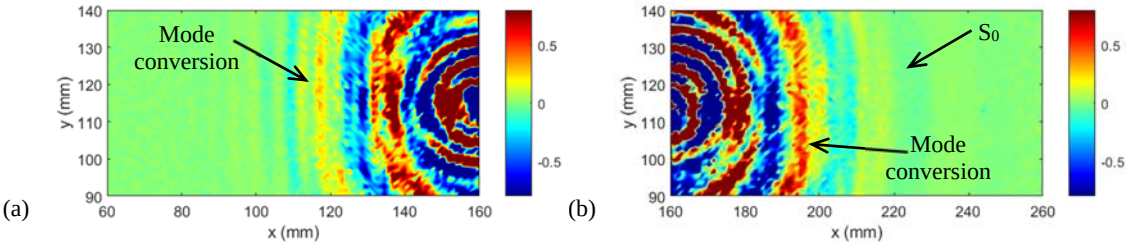

Figure 3 Wavefield snapshots at 22 μs of (a) wrinkle region, and (b) reference region

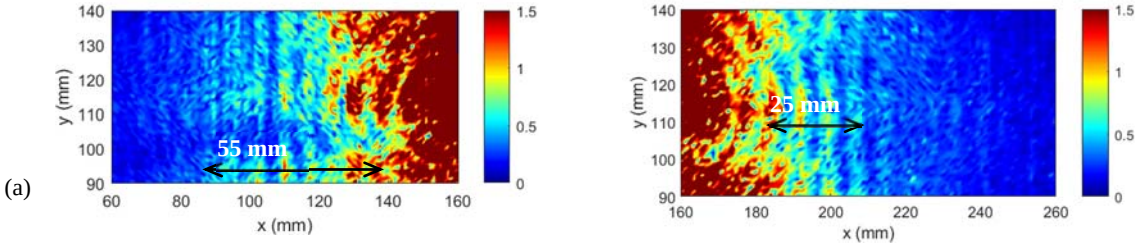

Figure 4 Energy field images: (a) wrinkle region, and (b) reference region

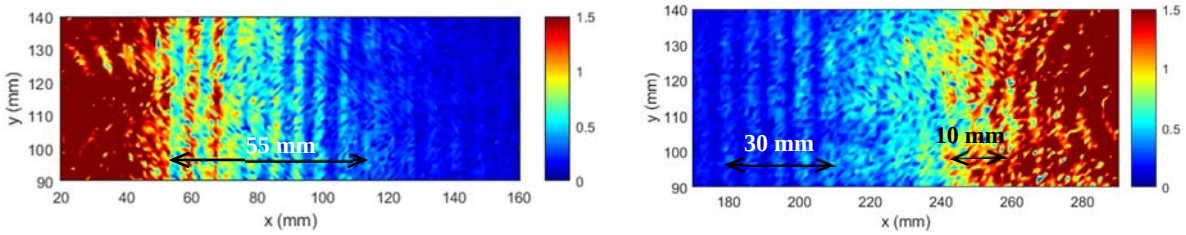

Figure 5 Energy field images. (a) wrinkle region with PZT attached at O_2, and (b) reference region with PZT attached at O_3

3.2 Case 2: delamination inspection

Delamination is evaluated in a curved composite plate in this case. The curved composite panel is manufactured by the National Aeronautics and Space Administration (NASA), which is shown in Figure 6. The height of the specimen is 101 mm, and the thickness is around 7 mm. The length of the specimen outside surface is 140 mm. Cartesian coordinates are used with the origin set at the left bottom corner on the top surface. The actuation setup is shown in Figure 6c with PZT actuator attached at O_1 and O_2 in order to inspect the specimen from different views. A 3-count toneburst at 150 kHz amplified to 50 V_{pp} is used as excitation for each test. Since the specimen is curved, the inspection is not the same as traditional SLDV scanning. The SLDV head is placed normally to the axis of symmetry of the panel as shown in Figure 6d, and the scanning angle effect is not considered. For each inspection, the scanning area covers the accessible surface of the specimen: around 100 mm × 90 mm for both sides. For each side, the inspection area differs slightly due to the curvature. Note that the scanning area is not identical to the real curved surface, and the measured wavefield is the shrink version of original wavefield in *x*-*z* plane due to the curvature. Note that the inspection is performed on the top surface of the panel.

The acquired time-space wavefields at 45 μs are plotted in Figure 7. Strong wave interactions are observed at same locations (marked with rectangle box) for both wavefields with PZT at O_1 and O_2. The energy intensity increases at those locations as well, indicating that waves trapped in the delamination and bounced back and forth. The damage location is detected at y=50 mm (delamination 1: D1) and y=80 mm (delamination 2: D2). In addition, the wave interactions at D1 is stronger than that at D2, indicating that D1 is closer to the top surface while D2 is further down away along the thickness

direction. Similar to case 1, energy field images are generated and presented in Figure 8 for both two inspections. The shape of D1 is revealed as a strip like profile: 10 mm by 6 mm, while D2 profile is not as clear as D1: with length about 60 mm along x direction. D2 might start at x=40 mm and end at x=100 mm where the two actuator locations are, thus that the actuated waves interact with it right after being excited, resulting the energy distribution shown in Figure 8.

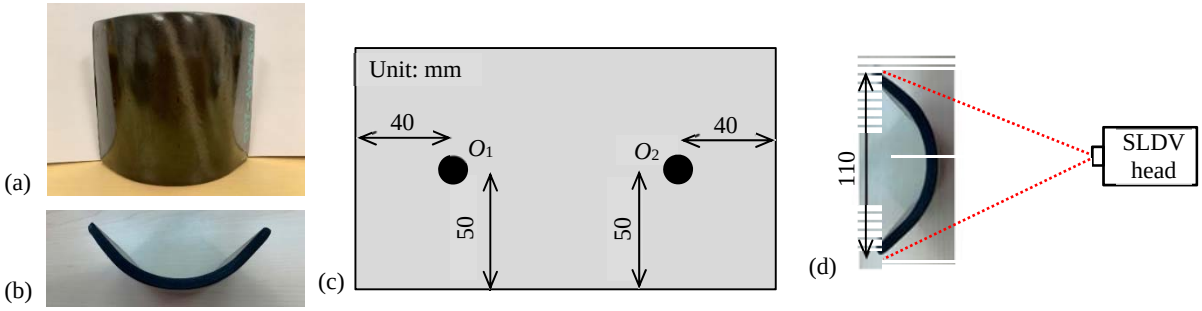

Figure 6 Inspection setup of the curved composite panel: (a) overall view of the panel, (b) side view showing the curvature, (c) inspection actuation scheme, and (d) inspection sensing setup

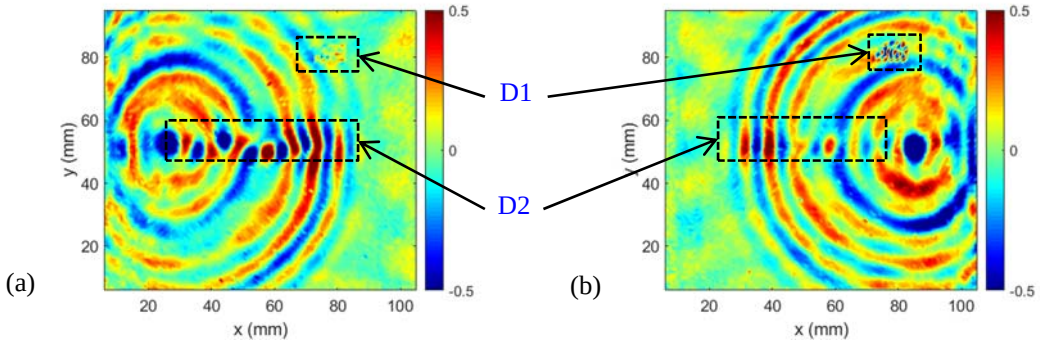

Figure 7 Wavefield snapshots at 45 μs of the top surface: (a) actuator at O_1, and (b) actuator at O_2

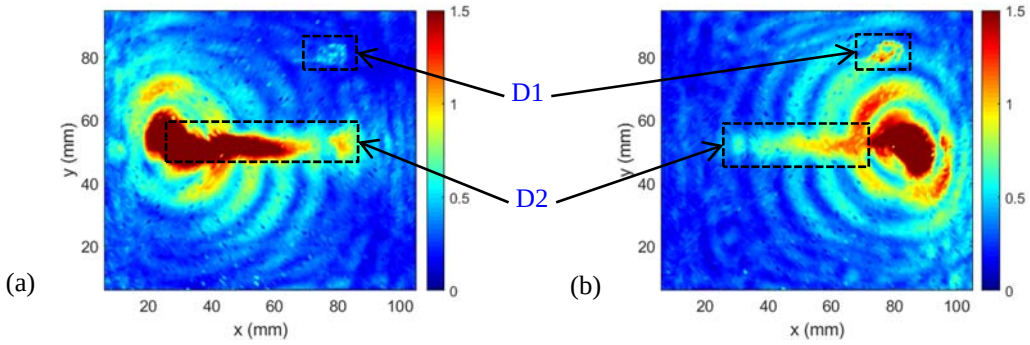

Figure 8 Energy field images of the top surface with: (a) actuator at O_1, and (b) actuator at O_2

4 CONCLUSIONS

In this paper, the capability of Lamb wave based NDE methods is established on composite panels with different geometries and with various embedded defects and damage. A nonintrusive PZT-SLDV Lamb wave NDE system is employed with honey as PZT actuation couplant instead of traditional adhesive while wipe-off reflective spray for SLDV signal enhancement instead of reflective tape. Two types of typical composite defect and damage are investigated using the nonintrusive PZT-SLDV system: case 1 wrinkle defects are evaluated in a flat composite panel while case 2 delamination is inspected in a curved composite panel. Mode conversion is observed when waves interact with wrinkles

while wave trapping occurred when waves encounter the delamination. Both the wrinkles and delamination are further evaluated and visualized through wavefield imaging methods and their shapes and locations are both quantified. Future work can be focused on exploration on inspection on the other side of the composite panels and adopt other wavefield imaging methods such as wavenumber imaging methods to better quantify the wrinkles and delamination.

5 ACKNOWLEDGEMENT

The material is based upon work supported by NASA under Award Nos. NNL09AA00A and 80LARC17C0004. Any opinions, findings, and conclusions or recommendations expressed in this material are those of the author(s) and do not necessarily reflect the views of the National Aeronautics and Space Administration.

6 REFERENCES

[1] H. W. Park, H. Sohn, K. H. Law *et al.*, "Time reversal active sensing for health monitoring of a composite plate," Journal of Sound and Vibration, 302(1-2), 50-66 (2007).

[2] A. Purekar, and D. Pines, "Damage detection in thin composite laminates using piezoelectric phased sensor arrays and guided Lamb wave interrogation," Journal of Intelligent Material Systems and Structures, 21(10), 995-1010 (2010).

[3] H. Sohn, D. Dutta, J. Yang *et al.*, "Automated detection of delamination and disbond from wavefield images obtained using a scanning laser vibrometer," Smart Materials and Structures, 20(4), 045017 (2011).

[4] K. E. Cramer, C. A. Leckey, P. A. Howell *et al.*, "Quantitative NDE of Composite Structures at NASA," (2015).

[5] P. D. Juarez, and C. A. Leckey, "Multi-frequency local wavenumber analysis and ply correlation of delamination damage," Ultrasonics, 62, 56-65 (2015).

[6] Z. Tian, L. Yu, and C. Leckey, "Delamination detection and quantification on laminated composite structures with Lamb waves and wavenumber analysis," Journal of Intelligent Material Systems and Structures, 26(13), 1723-1738 (2015).

[7] L. Yu, Z. Tian, X. Li *et al.*, "Core–skin debonding detection in honeycomb sandwich structures through guided wave wavefield analysis," Journal of Intelligent Material Systems and Structures, 30(9), 1306-1317 (2019).

[8] H. Sohn, D. Dutta, J.-Y. Yang *et al.*, "Delamination detection in composites through guided wave field image processing," Composites science and technology, 71(9), 1250-1256 (2011).

[9] Z. Tian, L. Yu, C. Leckey *et al.*, "Guided wave imaging for detection and evaluation of impact-induced delamination in composites," Smart Materials and Structures, 24(10), 105019 (2015).

[10] C. A. Leckey, and P. D. Juarez, "Ultrasonic NDE Simulation for Composite Manufacturing Defects," (2016).

[11] J. E. Michaels, [Ultrasonic wavefield imaging: Research tool or emerging NDE method?], (2017).

[12] L. Yu, Z. Tian, and C. A. Leckey, "Crack imaging and quantification in aluminum plates with guided wave wavenumber analysis methods," Ultrasonics, 62, 203-212 (2015).